Received: 7 November 2022 | Accepted: 30 March 2023

DOI: 10.1111/ddg.15113

ORIGINAL ARTICLE

Automatic body part identification in real-world clinical dermatological images using machine learning

Sebastian Sitaru[1] | **Talel Oueslati**[1] | **Maximilian C Schielein**[1] | **Johanna Weis**[1] | **Robert Kaczmarczyk**[1] | **Daniel Rueckert**[2,3] | **Tilo Biedermann**[1] | **Alexander Zink**[1,4]

[1]Technical University of Munich, School of Medicine, Department of Dermatology and Allergy, Munich, Germany

[2]Technical University of Munich, School of Medicine, Institute of AI and Informatics in Medicine, Munich, Germany

[3]Biomedical Image Analysis Group, Department of Computing, Imperial College London, London, UK

[4]Division of Dermatology and Venereology, Department of Medicine Solna, Karolinska Institutet, Stockholm, Sweden

Correspondence
Sebastian Sitaru, MD, Department of Dermatology and Allergy, Technical University of Munich, School of Medicine, Biedersteiner Strasse 29, 80802 Munich, Germany.
Email: sebastian.sitaru@tum.de

Summary

Background: Dermatological conditions are prevalent across all population subgroups. The affected body part is of importance to their diagnosis, therapy, and research. The automatic identification of body parts in dermatological clinical pictures could therefore improve clinical care by providing additional information for clinical decision-making algorithms, discovering hard-to-treat areas, and research by identifying new patterns of disease.

Patients and Methods: In this study, we used 6,219 labelled dermatological images from our clinical database, which were used to train and validate a convolutional neural network. As a use case, qualitative heatmaps for the body part distribution in common dermatological conditions was generated using this system.

Results: The algorithm reached a mean balanced accuracy of 89% (range 74.8%–96.5%). Non-melanoma skin cancer photos were mostly of the face and torso, while hotspots of eczema and psoriasis image distribution included the torso, legs, and hands.

Conclusions: The accuracy of this system is comparable to the best to-date published algorithms for image classification challenges, suggesting this algorithm could boost diagnosis, therapy, and research of dermatological conditions.

KEYWORDS
artificial intelligence, General dermatology, image classification, machine learning, medical dermatology

BACKGROUND

Skin conditions affect up to 70% of the world's population and can have a major impact on patients' quality of life and healthcare systems.[1–3] To help with triaging and diagnosing skin conditions, novel artificial intelligence methods such as deep learning are increasingly being researched. For example, the classification and segmentation of dermatological images, particularly those of skin cancers, are emerging as relevant and burgeoning topics in digital medicine.[4]

An integral part of dermatological skin findings is the location of skin lesions. Resources for dermatological differential diagnoses are often organized by body part.[5] Since some dermatological conditions preferentially affect certain body parts, the recognition of these predilection sites represents an important step in the dermatological diagnostic and therapeutic process. Some treatments are not indicated for certain body parts (e.g., polyhexanide on wounds on the nose and ear), while for some conditions the treatment must be escalated if certain body parts are

involved (e.g., shingles on the face).[6] Similarly, topical corticosteroids, the first-line anti-inflammatory agents, need to be chosen carefully based on the involved body parts to limit potential side effects.[7,8]

Classifying the body part of a dermatological image is not only of interest in clinical practice but also in translational research and public health studies. For many dermatological conditions, it is still not understood why certain body parts are preferentially affected.[9] Automatically classifying body parts based on clinical images can significantly accelerate research addressing this question. Automatic classification can also help to identify body parts associated with treatment-resistance faster and ultimately improve therapeutic outcomes. For example, lower legs and elbows were identified as hard-to-treat areas in psoriasis patients treated with biologics.[10]

Automatic classification of the body part can quickly provide this data point to physicians and algorithms, which, together with other data points such as patient age or skin type, can be used to improve diagnostic accuracy and conduct studies on a huge number of images at once. In fact, it was shown that combining data from images with metadata can significantly enhance a diagnostic algorithms' performance in dermatology.[11]

Algorithms for body part or organ recognition have so far been limited to data sources like computed tomography (CT) and X-ray images.[12–14]

While some algorithms have been developed to segment human body parts in still images and video, to the best of our knowledge no data on algorithms classifying real-world dermatological images based on specific body parts have been published to date. For example, algorithms have been developed to detect body parts when entire people are depicted, either in still photos or videos.[15–17] These algorithms, however, do not consider the high zoom levels and skin pathologies in dermatological clinical images and therefore are unsuited for classifying dermatological clinical pictures.

Collectively the current literature underlines an unmet need to develop automatic body part identification in clinical dermatological images. Therefore, in the present study we developed a deep-learning algorithm which aims to classify dermatological images from a clinical database to different body parts to improve the diagnosis, treatment, and research of dermatological conditions.

METHODS

Data source

Real-world clinical images of dermatological patients were used for this study. Clinical photographs are routinely taken at the department of Dermatology and Allergy at the School of Medicine, Technical University of Munich by a professional and dermatology-trained photographer. For each photo session, the physician fills out a form asking the date, diagnosis, and body parts to be photographed. Explicit written and informed patient consent for clinical and research purposes is obtained prior to each photo session. One photo session usually contains multiple photos, corresponding approximately to a single patient visit. One patient may have multiple photo sessions in our database depending on the disease and visit frequency. For this study, images from the database from 2006 to 2019 were selected.

Data pre-processing and labelling

For our dataset, we randomly selected 8,338 images on a per-image basis from our database. These images were manually assigned to one of twelve classes corresponding to a body part using a web frontend by one dermatology resident and two researchers with a background in medical research. Images which could not be accurately attributed to one body part, e.g., due to high zoom levels, were classified as "not classifiable" and disregarded for training and testing. After this sorting, 6,219 labelled images remained. Categories, their classification rules, and image counts are listed in Table 1. Common diagnoses were then grouped into 41 groups. Rare diagnoses (<2% images) and images with no diagnosis (e.g., cases where the diagnosis had still to be determined) were grouped into the "other" category.

Neural network layout

We used the Xception network architecture with no pre-trained weights.[18] Preliminary empirical studies showed that this constellation, in contrast to the other available networks in the keras framework, achieved the best performance. Two convolution layers and a dropout layer were added to prevent overfitting. Data were split randomly on a per-image basis to either training (80%) or test (20%) datasets, respectively. The network was trained using backpropagation and keras' implementation of the Adam algorithm as an optimizer.[19] A global learning rate of 0.001 was used, and the exponential decay rates were $\beta_1 = 0.9$ and $\beta_2 = 0.999$. An ε of 10^{-7} was applied. For training, data augmentation with keras' ImageDataGenerator was utilized. Each image was randomly zoomed with a range of [0.85; 1.15]. Each image was then randomly rotated with a range of [−15; +15] degrees. Lastly, images were randomly flipped horizontally with a probability of 0.5.

Performance calculation

The performance calculation of the network was performed using R v4.1.2 and the mltest library v1.0.1. The balanced

TABLE 1 Classes of images. This table shows the different body parts (classes), their classification criteria and the number of images in that group.

Name	Criteria	No. of images (%)
Anal/gluteal region (anal)	No more than 50% of image contains neighboring parts	379 (6.09%)
Arms (arms)	The arm(s) is/are clearly visible, hands may be depicted up to 50% of the hand	516 (8.3%)
Arms and hands (armsAndHands)	One or two arms and hands are fully depicted in the image	198 (3.18%)
Face (face)	The head is rotated in such a way that all facial features (eyes, nose, mouth) are visible	968 (15.57%)
Male genitals (genitalsMale)	No more than 50% of image contains neighboring parts	497 (7.99%)
Feet (feet)	Feet are clearly visible, but no more than 50% of the calf is depicted	422 (6.79%)
Female genitals (genitalsFemale)	No more than 50% of image contains neighboring parts	118 (1.9%)
Hands (hands)	One or two hands are clearly visible, and arms can be depicted up to the middle of the forearm	726 (11.67%)
Head (head)	The head is depicted, but criteria for face are not fulfilled	164 (2.64%)
Legs (legs)	The legs are clearly visible, feet may be depicted up to 50% of the forefoot	854 (13.73%)
Legs and feet (legsAndFeet)	One or two legs and feet are clearly visible	223 (3.59%)
Torso (torso)	The body is rotated in such a way that features of the front or back torso (umbilicus, breasts, back) are visible	1154 (18.56%)
Total	6219 (100%)	
Other	Images not meeting criteria specified above, e.g., due to zoom level	2119

accuracy was calculated as (TP / (TP+FN)+TN / (TN+FP)) / 2, where TP = true positives, FN = false negatives, TN = true negatives, and FP = false positives.

Evaluation of body part distribution per diagnosis

The algorithm was run on a clinical database consisting of around 200,000 images, and diagnoses were grouped as described in the section "data pre-processing and labelling". A 100 × 100 coordinate grid was created in R software. A picture of a human outline was overlayed and the different body parts were assigned to points representing their approximate physical location on the body map. The percentages of images were assigned to these points. Arms, legs, hands, and feet were mirrored to the other side, respectively. The values of the remaining points on the coordinate system were then filled using the Inverse Distance Weighting interpolation algorithm.

Data protection & ethics

All subjects provided written informed consent for the pictures to be used for research purposes. According to the Bavarian hospital law (BayKrG) secondary patient data can be leveraged for research purposes. Since this applies to the project and in addition no human or animal subjects were directly involved, an additional ethics approval was not needed for this project. The data was not transmitted to any third-party service or machine.

RESULTS

Dataset description

In our final dataset of 6,219 images, the mean image count per class was 518 and the median count 459 images. The standard deviation was 339. The lowest number of images were in the female genitals class with 118 images (1.9%), the highest in the torso class with 1,154 (18.6%). The distribution of the most common diagnoses, excluding the "other" category, can be seen in Table 2. The most common diagnoses were eczema (11.1%, 689 images), psoriasis (6.6%, 409 images), hypereosinophilia (3.6%, 222 images), and non-melanoma skin cancer (NMSC, 3.2%, 201 images). Most images were of the "other" diagnosis group (57.1%, 3,551 images). There was no clear diagnosis for 8.9% of images (n = 552).

TABLE 2 Image counts in terms of diagnoses. This table shows the biggest diagnostic groups in the test and train dataset. The "other" class includes images with diagnoses that make up <2% of the total dataset. Percentages are listed column-wise.

	Test	Train	Total
Acne	49 (3.9%)	86 (1.7%)	135 (2.2%)
Eczema	137 (11%)	552 (11.1%)	689 (11.1%)
HES	57 (4.6%)	165 (3.3%)	222 (3.6%)
Lymphoma	35 (2.8%)	125 (2.5%)	160 (2.6%)
Mastocytosis	26 (2.1%)	120 (2.4%)	146 (2.3%)
Melanoma	33 (2.6%)	121 (2.4%)	154 (2.5%)
ND	106 (8.5%)	446 (9%)	552 (8.9%)
NMSC	37 (3%)	164 (3.3%)	201 (3.2%)
Other	682 (54.6%)	2869 (57.7%)	3551 (57.1%)
Psoriasis	87 (7%)	322 (6.5%)	409 (6.6%)
Total	1249 (100%)	4970 (100%)	6219 (100%)

Abbr.: HES, hypereosinophilic syndrome; ND, no diagnosis; NMSC, non-melanoma skin cancer

TABLE 3 Model performance by body part class. This table shows the models' performance metrics grouped by the different body parts.

	Balanced accuracy	Sensitivity	Specificity	F1
Anal	0.796	0.610	0.982	0.662
Arms	0.857	0.728	0.985	0.777
ArmsAndHands	0.947	0.900	0.994	0.878
Face	0.965	0.949	0.981	0.933
Feet	0.865	0.741	0.988	0.788
GenitalsFemale	0.748	0.500	0.996	0.595
GenitalsMale	0.927	0.871	0.984	0.853
Hands	0.963	0.952	0.974	0.900
Head	0.845	0.697	0.993	0.730
Legs	0.885	0.802	0.967	0.809
LegsAndFeet	0.927	0.867	0.986	0.796
Torso	0.953	0.935	0.971	0.916
Mean	0.890	0.796	0.984	0.803

Performance

Overall mean accuracy was 89.0% (standard deviation ± 7%). The mean sensitivity was 79.6% (± 14.4%), the mean specificity 98.4% (± 0.9%), and the mean F1 score 0.80 (± 0.11). As shown in Table 3, the highest balanced accuracy was achieved for the face (96.5%), hands (96.34%), and torso (95.3%) classes. The lowest accuracy was achieved for the female genitals (74.8%), anogenital region (79.64%), and head excluding face (84.5%) classes. Highest sensitivity was achieved for the hands (95.2%) and the lowest for female genitals (50%). The highest specificity was observed for female genitals (99.6%) and the lowest specificity for legs (98.7%). As observed in the confusion matrix (Figure 1), most images in most classes were assigned the correct label. Common errors included the mislabeling of arms as legs (n = 11), hands as feet (n = 11), and anogenital areas as the face (n = 10).

Body part distribution per diagnosis

To test a possible application of our algorithm, we analyzed the body part distribution for eczema, psoriasis, and NMSC, three of the most common diagnosis groups in our whole database. As shown in Figure 2, for eczema (n = 16,053 images) most images were of the head, arms, and torso. For psoriasis (n = 11,724 images), hotspots were the torso, legs, and arms. For NMSC (n = 1,692), most images were of the face.

DISCUSSION

In this study, we present a novel algorithm for classifying body parts in dermatological clinical images. The large dataset of around 6,000 manually labeled clinical images was slightly class-imbalanced, with the difference between the smallest and largest classes being around 1,000 images. About half of the images were of the three largest diagnosis classes: eczema, psoriasis, and NMSC. The remaining images were of rarer conditions in the "other" class. The algorithm achieved a high accuracy of 89%, with an excellent specificity of around 98% and a very good sensitivity of around 80%.

Performance interpretation

This algorithm represents an attempt at the automated analysis of depicted body parts in dermatological images. Algorithms for segmenting and classifying body parts in images showing the entire body have been described before.[20] Furthermore, machine learning (ML)-based automated calculation of the psoriasis area severity index (PASI) in dermatological images was recently described.[21] However, the classification of one image to one body part has not been described to date.

Regarding performance, the accuracy of the Xception net in the ImageNet classification challenge was 79%. The best reported performance to-date in the ImageNet challenge is around 90%.[22] The segmentation algorithms mentioned in the introduction achieved accuracies of 70–80% depending on the dataset.[12–14] Our algorithm showed a mean accuracy of 89%.

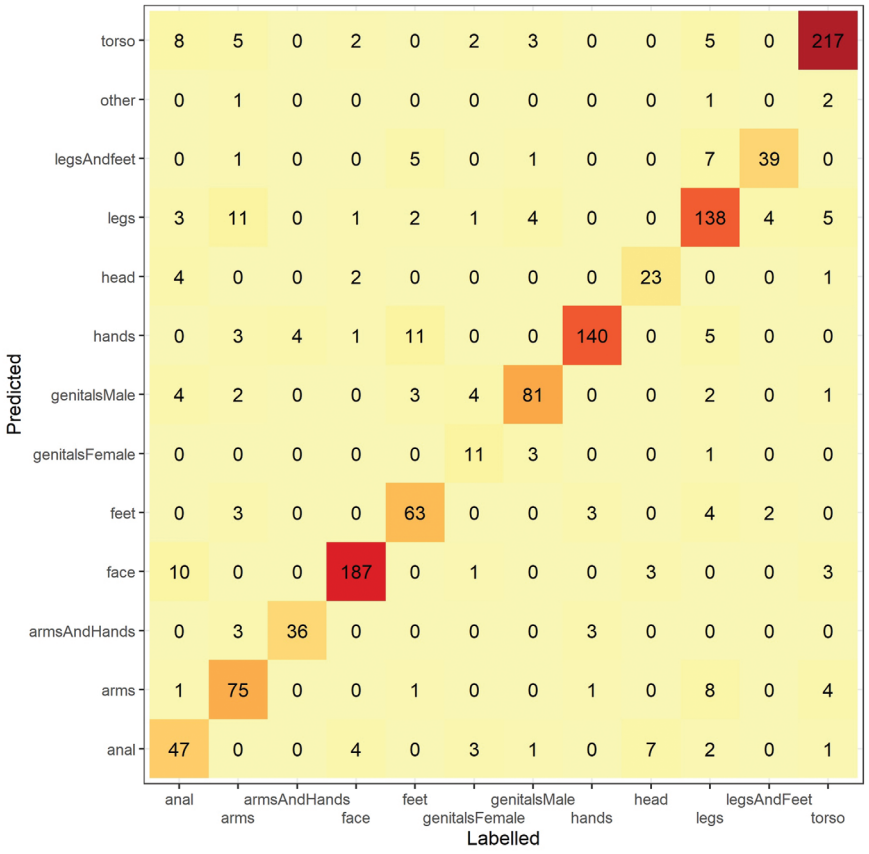

FIGURE 1 Confusion matrix. This figure shows a confusion matrix of the algorithm's validation. The labelled body part is plotted on the x-axis and the predicted body part is plotted on the y-axis. The numbers are absolute numbers of the corresponding images. The color coding is a linear representation of these absolute numbers (from yellow to red). Most predicted classes corresponded to the ground truth. Common mislabelings were images of arms labeled as legs (n = 11), hands as feet (n = 11), and the anogenital area as the face (n = 10).

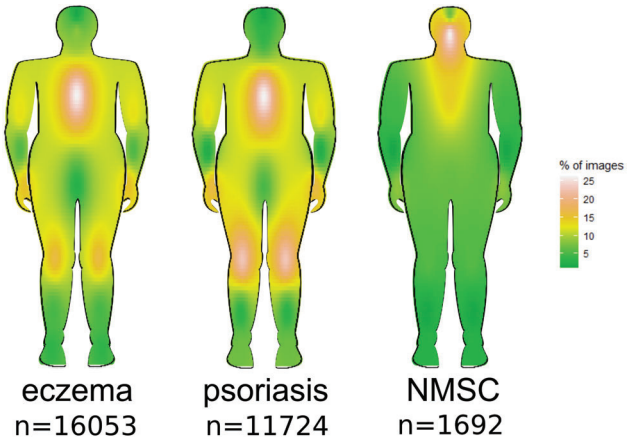

FIGURE 2 Image body part distribution for eczema, psoriasis, NMSC. This figure shows the distribution of images of the eczema, psoriasis, and non-melanoma skin cancer (NMSC) diagnosis groups as qualitative heatmaps. The color qualitatively represents the percentage of images in a given body area.

Distribution of affected body parts in eczema, psoriasis, and NMSC

Non-melanoma skin cancer appears to mostly affect the face and torso, which corresponds to typically sun-exposed areas (Figure 2). For psoriasis and eczema, most photographed body parts were the torso, legs, and hands (Figure 2). Psoriasis is reported in the literature to usually affect the extensor areas, scalp, anogenital region, and umbilicus.[23,24] For eczema, typically affected areas include the flexural areas and, particularly for adults, the head and neck area.[25] Discrepancies can therefore be observed for both diseases. For psoriasis, the head and face were seemingly nearly never photographed, whereas the torso was photographed frequently. Similarly for eczema, the torso, which was not mentioned frequently as an affected site in the literature, was repeatedly photographed. One possible interpretation of this discrepancy is that the torso may represent an additional but lesser known site of predilection for these two diseases.

Limitations

Limitations of our algorithm include a class imbalance, biases regarding the diagnoses, and the inability to classify images as non-classifiable. In the female genitals class, only 118 images were labelled, whereas in the torso class 1,154 were labelled. This represents a class imbalance and a potential factor negatively impacting algorithm performance.[26] The imbalance was corrected using data augmentation as described in the methodology. This class imbalance may reflect clinical routine and patient sensibilities, as patients may be less receptive to having photographs of their anogenital region taken than of other

body parts. Therefore, it is likely that in other databases, this group is also underrepresented and too small for meaningful research.

Bias regarding diagnoses must be considered, as some conditions are not as routinely photographed as others. Less photographed skin conditions include actinic keratosis and other skin cancers, which are therefore underrepresented in our dataset when compared to the prevalence in actual dermatological routine. Nevertheless, our dataset still offers a wide range of common and uncommon diagnoses (Table 2). Especially images of the three most common dermatological conditions, eczema, psoriasis, and NMSC, were plentiful. This bias therefore should not limit the algorithm's performance in real-world settings as well as for uncommon dermatological conditions.

Our algorithm does not yet include a validated method to classify non-classifiable images (e.g., because of high zoom levels, no skin being shown or multiple body sites being shown). This could be implemented in the future using temperature scaling in the activation function of the last layer and a cut-off of the resulting probability estimate.[27] In addition, a more accurate classification of, for example, the flexor and extensor sides of an extremity could add considerable value for some dermatological diseases.

Overall, for the analysis of body parts using this technique, it should be emphasized that biases exist depending on diagnoses and depicted body parts because of the data quality provided by a given database.

Conclusion and outlook

In conclusion, we have presented the to date first algorithm to accurately label the body part of clinical dermatological images of both common and rare diagnoses. Applications of this algorithm include support of clinical practice by facilitating diagnosis and treatment planning. Furthermore, this algorithm may act as a basis for future and more sophisticated machine-learning algorithms for e.g., diagnostic triage, as many dermatological conditions are defined by their morphological characteristics and predilection sites. Similarly, the analyses of lesser-known predilection sites or treatment-resistant locations in dermatological research, such as presented for psoriasis in the introduction, could be automated using this algorithm. For example, this study was able to demonstrate for eczema and psoriasis discrepancies between the distribution of frequently photographed body parts and the frequency of affected locations reported in the literature. Furthermore, the automated analysis of body parts could help discover unmet needs in the treatment, like was demonstrated for genital involvement of psoriasis.[28,29]

For less well understood conditions, further insights into their pathophysiology and subsequently treatment may be gained by subgrouping them by affected body part (e.g., the differences between nummular eczema on the trunk and the extremities).

Also, integration of such an algorithm with three-dimensional body scanners is a promising avenue for both clinical practice and dermatological research. These body scanners offer a fast and objective way of obtaining skin findings and can be used for example for automated scoring of skin diseases.[30] It was shown that involvement of a sensitive body area, like genitals, leads to decreased quality of life in dermatological conditions.[28] Therefore, the affected body part needs to be analyzed and included in scores for dermatological conditions to get the most accurate representation of disease severity.

To improve performance of this algorithm, future studies should include a larger and more balanced dataset and a "non-classifiable" class. Also, it could be extended to distinguish the exact location of a certain body region (e.g., the front or back of the torso) or a combination of different body parts in a multi-label classification setting (e.g., images which show the torso and both arms). If data sharing between multiple sites for training is not possible, as is often the case with patient images, an integration of this algorithm with swarm learning is possible.[31] With swarm learning, no original data is shared between the nodes while training the algorithm together. Finally, to better validate the performance of this body part classification algorithm, future evaluations with external datasets should be conducted.

AUTHOR CONTRIBUTIONS

S.S., M.S., T.O., and A.Z. conceived the idea for this project. T.O., S.S. and R.K. wrote the code. S.S., M.S. and J.W. labelled the data. T.O. and S.S. trained the network. S.S. analyzed the data and wrote the manuscript with input from all authors. T.B. and A.Z. supervised the project from a medical perspective, D.R. supervised the project from an informatics perspective.

The patients in this manuscript have given written informed consent to publication of their case details.

DATA AVAILABILITY

The Python scripts used to pre-process the data, train the network, and validate it can be found on GitHub: https://github.com/ssitaru/bodypart-id. The original data (patient pictures) cannot be provided online.

ACKNOWLEDGEMENT

Open access funding enabled and organized by Projekt DEAL.

CONFLICT OF INTEREST

S.S.: speaker's honoraria from Amgen. M.C.S: Consulting fees from LEO Pharma; speaker's honoraria from Novartis, Janssen Cilag, LEO Pharma; current employee of Novartis. T.B.: Consulting fees from AbbVie, Alk Abelló, Celgene-BMS,

Lilly Deutschland GmbH, Mylan, Novartis, Phadia-Thermo Fisher, p-95 for Curevac, Sanofi-Genzyme, Regeneron, Viatris. A.Z.: unrestricted research grant from LEO Pharma and Novartis Pharma in the field of atopic dermatitis and psoriasis; advisor and/or received speaker's honoraria of the following companies related to eczema and psoriasis: Eli Lilly, Leo Pharma, Novartis Pharma, Pfizer, Sanofi-Aventis, UCB, Janssen Cilag; member of the German Society of Dermatology and leader of the Digital Dermatology group within this society.

REFERENCES

1. Hay RJ, Johns NE, Williams HC, et al. The Global Burden of Skin Disease in 2010: An Analysis of the Prevalence and Impact of Skin Conditions. *J Invest Dermatol*. 2014;134(6):1527-1534 .
2. Schielein MC, Tizek L, Ziehfreund S, et al. Stigmatization caused by hair loss – a systematic literature review. *J Dtsch Dermatol Ges*. 2020;18(12):1357-1368.
3. Tizek L, Schielein M C, Seifert F, et al. Skin diseases are more common than we think: screening results of an unreferred population at the Munich Oktoberfest. *J Eur Acad Dermatol Venereol*. 2019;33(7):1421-1428.
4. Efimenko M, Ignatev A, Koshechkin K. Review of medical image recognition technologies to detect melanomas using neural networks. *BMC Bioinformatics*. 2020;21(Suppl 11):270.
5. Ashton R, Leppard B. *Differential Diagnosis in Dermatology*. CRC Press, 2020.
6. Gross G E, Eisert L, Doerr HW, et al. S2k-Leitlinie zur Diagnostik und Therapie des Zoster und der Postzosterneuralgie. *GMS Infect Dis*. 2020;8:Doc01
7. Giannotti B. Current Treatment Guidelines for Topical Corticosteroids: *Drugs*. 1988;36(Supplement 5):9-14.
8. Mori M, Pimpinelli N, Giannotti B. Topical Corticosteroids and Unwanted Local Effects: Improving the Benefit/Risk Ratio. *Drug Saf*. 1994;10(5):406-412.
9. Smolle J. [Predilection sites of the skin]. *J Dtsch Dermatol Ges*. 2003;1(8):646-651;quiz 652,654
10. Hjuler K F, Iversen L, Rasmussen MK, et al. Localization of treatment-resistant areas in patients with psoriasis on biologics. *Br J Dermatol*. 2019;181(2):332-337.
11. Liu Y, Jain A, Eng C, et al. A deep learning system for differential diagnosis of skin diseases. *Nat Med*. 2020;26(6):900-908.
12. Dicken V, Lindow B, Bornemann L, et al. Rapid image recognition of body parts scanned in computed tomography datasets. *Int J Comput Assist Radiol Surg*. 2010;5:527-535.
13. Andrási E, Varga I, Dózsa A, et al. Classification of human brain parts using pattern recognition based on inductively coupled plasma atomic emission spectroscopy and instrumental neutron activation analysis. *Chemom Intell Lab Syst*. 1994;22(1):107-114.
14. Zhou X. Automatic Segmentation of Multiple Organs on 3D CT Images by Using Deep Learning Approaches. *Adv Exp Med Biol*. 2020;1213:135-147.
15. Shebiah R N, Sangari AA. Classification of human body parts using histogram of oriented gradients. in *2019 5th International Conference on Advanced Computing & Communication Systems (ICACCS)*. 2019:958-961.
16. Argenziano G, Soyer HP, Chimenti S, et al. Dermoscopy of pigmented skin lesions: results of a consensus meeting via the Internet. *J Am Acad Dermatol*. 2003;48(5):679-693.
17. Goutsu Y, Takano W, Nakamura Y. Classification of Multi-class Daily Human Motion using Discriminative Body Parts and Sentence Descriptions. *Int J Comput Vis*. 2018;126(5):495-514.
18. Chollet F. Xception: Deep Learning with Depthwise Separable Convolutions. *ArXiv161002357 Cs* 2017.
19. Kingma DP, Ba J. Adam: A Method for Stochastic Optimization. *ArXiv14126980 Cs* 2017.
20. Oliveira GL, Valada A, Bollen C, et al. Deep learning for human part discovery in images. *IEEE International Conference on Robotics and Automation (ICRA)*, Stockholm, Sweden, 2016;1634-1641.
21. Schaap MJ, Cardozo NJ, Patel A, et al. Image-based automated Psoriasis Area Severity Index scoring by Convolutional Neural Networks. *J Eur Acad Dermatol Venereol*. 2022;36(1):68-75.
22. Dai Z, Liu H, Le QV, Tan M. CoAtNet: Marrying Convolution and Attention for All Data Sizes. *ArXiv210604803 Cs* 2021.
23. Griffiths CE, Barker JN. Pathogenesis and clinical features of psoriasis. *Lancet*. 2007;370(9583):263-271.
24. Mrowietz U, Prinz JC. Psoriasis. In: Plewig G, Ruzicka T, Kaufmann R, Hertl M. (eds) *Braun-Falco's Dermatologie, Venerologie und Allergologie. Springer Reference Medizin*. Berlin, Heidelberg: Springer. 2018:677-702.
25. Homey B, Ruzicka T, Wollenberg A. Atopisches Ekzem. In: Plewig G, Ruzicka T, Kaufmann R, Hertl M. (eds) *Braun-Falco's Dermatologie, Venerologie und Allergologie*. Berlin, Heidelberg: Springer Reference Medizin, Springer. 2018:549-568.
26. Buda M, Maki A, Mazurowski MA. A systematic study of the class imbalance problem in convolutional neural networks. *Neural Netw*. 2018;106:249-259
27. Guo C, Pleiss G, Sun Y, Weinberger KQ. On Calibration of Modern Neural Networks. *ArXiv170604599 Cs* 2017.
28. Schielein MC, Tizek L, Schuster B, et al. Genital psoriasis and associated factors of sexual avoidance – a people-centered cross-sectional study in Germany. *Acta Derm Venereol*. 2020;100(10):adv00151.
29. Ryan C. Genital psoriasis: the failure of dermatologists to identify genital involvement. *Br J Dermatol*. 2019;180(3):460-461.
30. Rutjes C, Torrano J, Soyer HP. A 3D total-body photography research network: the Australian experiment. *Hautarzt*. 2022;73:236-240.
31. Warnat-Herresthal S, Schultze H, Shastry K L, et al. Swarm Learning for decentralized and confidential clinical machine learning. *Nature*. 2021;594(7862):265-270.

How to cite this article: Sitaru S, Oueslati T, Schielein MC, et al. Automatic body part identification in real-world clinical dermatological images using machine learning. *JDDG: Journal der Deutschen Dermatologischen Gesellschaft*. 2023;21:863–869.
https://doi.org/10.1111/ddg.15113